Coalescence of Bubbles with Mobile Interfaces in Water

Bo Liu, Rogerio Manica, and Qingxia Liu*
Department of Chemical and Materials Engineering, University of Alberta, Edmonton T6G 1H9, Canada

Evert Klaseboer
Institute of High Performance Computing, 1 Fusionopolis Way, Singapore 138632

Zhenghe Xu
Department of Chemical and Materials Engineering, University of Alberta, Edmonton T6G 1H9, Canada
and Department of Materials Science and Engineering, Southern University of Science and Technology, Shenzhen 518055, China

Guangyuan Xie
Department of Chemical Engineering, China University of Mining and Technology, Xuzhou 221116, China

(Received 31 December 2018; revised manuscript received 11 February 2019; published 14 May 2019)

The fluid flow inside a thin liquid film can be dramatically modified by the hydrodynamic boundary condition at the interfaces. Aqueous systems can be easily contaminated by trace amounts of impurities, rendering the air-liquid interface immobile, thereby significantly resisting the fluid flow. Using high speed interferometry, rapid thinning of the liquid film, on the order of the collision speed, was observed between two fast approaching air bubbles in water, indicating negligible resistance and a fully mobile boundary condition at the air-water interface. By adding trace amounts of surfactants that changed the interfacial tension by 10^{-4} N/m, a transition from mobile to immobile was observed. This provides a fundamental explanation why the bubble coalescence time can vary by over 3 orders of magnitude.

DOI: 10.1103/PhysRevLett.122.194501

When two air bubbles collide with each other, they may bounce and keep their original volume or merge into a larger one. The collision of air bubbles plays a pivotal role in many fields including oil and gas extraction, mineral flotation, and water purification, even though the expected outcome varies with industries. For example, large bubbles are desired for drag reduction [1], whereas microbubbles are beneficial for froth flotation [2]. Bubble coalescence occurs when the trapped thin liquid film reaches its critical rupture thickness, typically in the order of 50 nm [3,4]. Within a dynamic collision process with limited time (∼0.01–0.12 s) [5], the crucial factor determining the bubble collision is the film thinning rate [3], which is influenced by bubble size, collision velocity, nonsymmetric drainage, and most importantly, the hydrodynamic boundary condition at the interface [3,4,6–9]. The latter may be tangentially immobile (zero tangential velocity at the air-liquid interface due to the presence of contaminants or surfactants) or fully mobile (when the air-liquid interface cannot sustain any shear stress, as is the case of bubbles in pure water).

The mobility of air-liquid interfaces has been utilized for drag reduction by using superhydrophobic surfaces in microfluidics [10,11] or covering falling spheres with an air layer [12]. Theoretically, the film thinning rate between two bubbles with mobile interfaces can be 3 or 4 orders of magnitude faster than that with tangentially immobile interfaces [13]. Though the existence of mobile air-water interfaces in bubble coalescence is still controversial, experiments have found instances of rapid bubble coalescence in milliseconds [3,14], which was hypothesized to be a result of interface mobility without any evidence on a film level. However, direct observations of the spatiotemporal thinning of the thin liquid film using interferometry, when compared with theoretical prediction, have thus far consistently confirmed the immobile air-water boundary condition. Experimental data were obtained for the interaction between an air bubble and hydrophilic or hydrophobic surfaces over a wide range of Reynolds numbers [15–18], and between two bubbles in quasistatic or dynamic conditions [4,7,19]. Phenomenological features of the thinning film, including the inversion of curvature (dimple) and the dynamic evolution of the dimple profile, agreed well with theoretical prediction assuming the immobile boundary condition [15]. Even freshly generated bubbles with fully mobile surfaces during the rise in bulk exhibited an immobile boundary condition when colliding with a solid surface [16,17]. The discrepancy between experiments leaves a gap in researchers' understanding of air-water interfaces.

In this Letter, we report bubble collision experiments using high speed interferometric images that provide

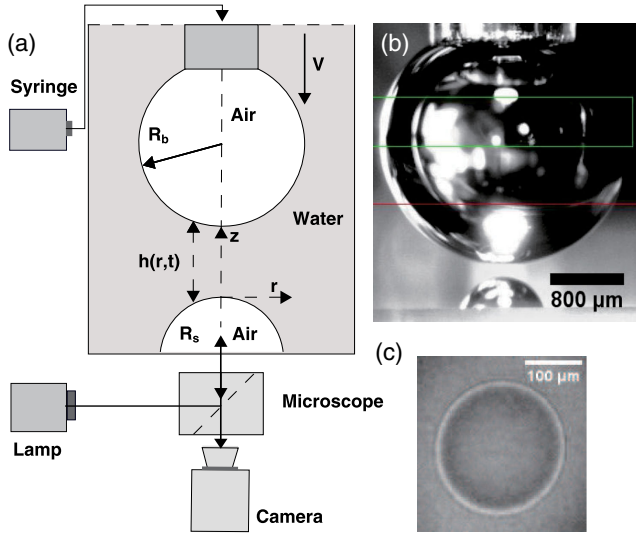

FIG. 1. (a) Schematic of the experimental setup. A bubble of radius $R_b = 1.2$ mm was held at the glass capillary orifice, whereas another bubble of radius R_s was immobilized on a hydrophobic silica surface. The capillary was driven downward by a speaker diaphragm at the velocity V to achieve collision between the bubbles. A high-speed camera connected to an inverted microscope was used to record the interference fringes. (b) Side view illustration of the bubbles, where lines are used to monitor top bubble size and position. (c) A snapshot of the interference fringes obtained between two colliding bubbles ($R_s = 0.79$ mm, $V = 28$ mm/s, and 5 mM SDS).

quantitative information on the thinning behavior and the rupture of the thin liquid film trapped between two bubbles. Analysis of the interferometry fringes revealed a rapid coalescence process within a few milliseconds, which is 3 or 4 orders of magnitude faster than most reported data for immobile drainage. This observation can be characterized using a lubrication model that assumes a tangentially mobile hydrodynamic boundary condition at the air-water interfaces [20–22]. We further show that a minor amount of surfactant that changes the interfacial tension in the order of 10^{-4} N/m will be enough to alter the hydrodynamic boundary condition significantly. The transition is likely associated with the balance of shear and Marangoni stresses at the interface.

A schematic of the dynamic force apparatus [4,18] is shown in Fig. 1(a). The experiments were conducted in a glass vessel filled with Milli-Q purified water or surfactant solutions. By injecting ambient air from a gas-tight syringe into a capillary tube, we generated and held a bubble ($R_b = 1.2$ mm) at the orifice of the capillary, while another bubble (R_s is between 400 and 850 μm) was immobilized on a hydrophobic fused silica glass surface (contact angle ≈100°, treated by Octadecyltrichlorosilane). Because the air-water interface is known to be easily immobilized by a tiny amount of impurities [6,8], a thorough cleaning procedure was adopted and experiments were performed quickly after the bubbles were generated (within 5 min). The glass vessel, the capillary tube, and the hydrophobic silica surface were rinsed thoroughly before each set of experiments. The liquid in the glass vessel, which was open to air, was changed hourly to avoid contamination from the ambient air. Moreover, the bottom bubble was formed by the breakage of a capillary bridge (see Supplemental Material for details [23]).

The process was monitored by a side view CCD camera so that the bubbles could be carefully aligned to achieve head-to-head collision [see Fig. 1(b)]. The top bubble was pushed towards the bottom one by a speaker diaphragm at the controlled collision velocity V between 0.5 and 50 mm/s. The deformation of the bubble due to its acceleration and movement was small or negligible at the speeds used in this study. The thinning and rupture of the thin liquid film trapped between the bubbles was directly observed by an inverted microscope (Carl Zeiss Axiovert 100) through the transparent silica glass and recorded by a high-speed camera (Photron SA4, 40 000 frames/s). The lighting was achieved by a high intensity mercury lamp (X-Cite 120Q). The spatial resolution was approximately 2 μm/pixel. An example of recorded interferometric fringes is shown in Fig. 1(c).

Figure 2(a) shows a sequence of interference fringes leading up to the rupture of the thin liquid film. The rapid evolution of interference fringes indicating fast film thinning behavior within 3 ms is shown in snapshots 1 to 4, followed by a dark area (snapshot 5) marking the coalescence of the bubbles (film ruptured). An axisymmetric

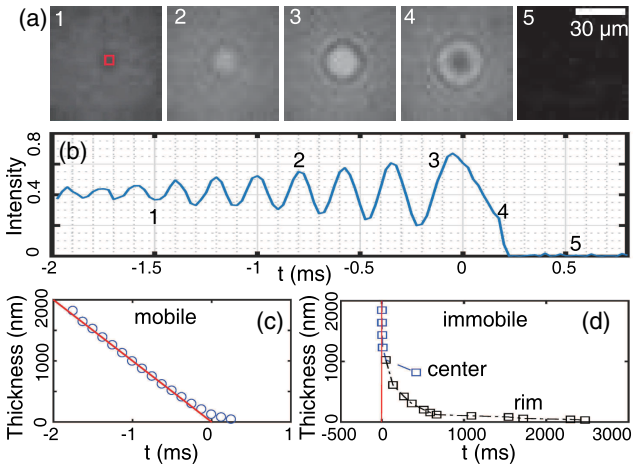

FIG. 2. (a) Snapshots of the interference fringes in a time sequence obtained between two colliding bubbles ($R_s = 0.73$ mm, $V = 1$ mm/s). (b) Evolution of the light intensity at the film center marked by the red square (2×2 pixels, $\sim 4 \times 4$ μm^2), from which we obtained (c) time evolution of the film thickness (circles) compared with approaching undeformed bubbles (straight line). (d) Thin film drainage with immobile air water interfaces ($R_s = 0.55$ mm, $V = 1$ mm/s). Before collision, the bubbles were left in bulk for over 60 min so that the interfaces were contaminated and immobilized.

drainage behavior of the liquid film can be deduced from the interference fringes. In experiments in clean systems, there was no clear evidence of the inversion of the thin liquid film or "dimple" formation, which is typically present for reported experiments with immobile boundary conditions [4,17,24]. Furthermore, the film radius was smaller than 20 μm during the drainage process, whereas it would easily exceed 100 μm with immobilized air-water interfaces. This result suggests a very small hydrodynamic resistance during the drainage process.

The evolution of the light intensity in the central area of the film is plotted in Fig. 2(b), from which the time evolution of the film thickness shown in Fig. 2(c) was obtained. We define the time $t = 0$ as the point when the two nondeformable bubbles would have touched at a given applied approach speed, so the "coalescence time" can be defined as the time taken from this point to film rupture. In Fig. 2(c), the experimental result revealed that the two interfaces approached each other from 2000 to 100 nm at the same speed as the bubble approach velocity, followed by a gradual decrease in the thinning rate until rupture at around 30 nm, resulting in a coalescence time of 0.2 ms. This result further confirmed the low resistance at the air-water interfaces. In contrast, as shown in Fig. 2(d), the drainage slowed down dramatically for the same process with immobile air-water interfaces, in which the coalescence was delayed by over 2000 ms with the dimple formation at the film thickness of ~1 μm where the film at the center became thicker than at the rim.

In Fig. 3(a) we show the evolution of film thickness at different collision speeds ranging from 0.5 to 2.8 mm/s. The film thinning rate increases with collision speed. More specifically, the experimental film thinning rates from film thickness 2000 to ~100 nm followed the respective experimental approach speed ($-dh/dt = V$) of the bubbles. This relationship agreed better at higher velocities than at lower ones, where the experimental thinning rate was slightly slower in some cases. Furthermore, there was a consistent slowdown of the film thinning rate when the film thickness reached ~100 nm.

Based on the above results two questions can be asked: (i) What is the physics behind the rapid thinning behavior with negligible resistance? (ii) What is the reason for the observed slowdown of the film thinning rate at $h \sim 100$ nm? To answer these questions, we compared these experimental results with the predictions from a constant velocity model that assumes mobile fluid-fluid interfaces [20–23]. In this model, the liquid drainage is described by lubrication theory, while the flow inside the bubble is described by Stokes flow. The interfacial velocity U is determined by the continuity of the tangential shear stress across the interface ($\tau_b = \tau_f$), which arises from film liquid flow $\tau_f = \mu \partial u/\partial z|_{z=z^+}$, and the bubble air flow $\tau_b = \mu_{\text{air}} \partial u/\partial z|_{z=z^-}$ (with z^+ and z^- indicating positions at the liquid and air sides of the interface, respectively).

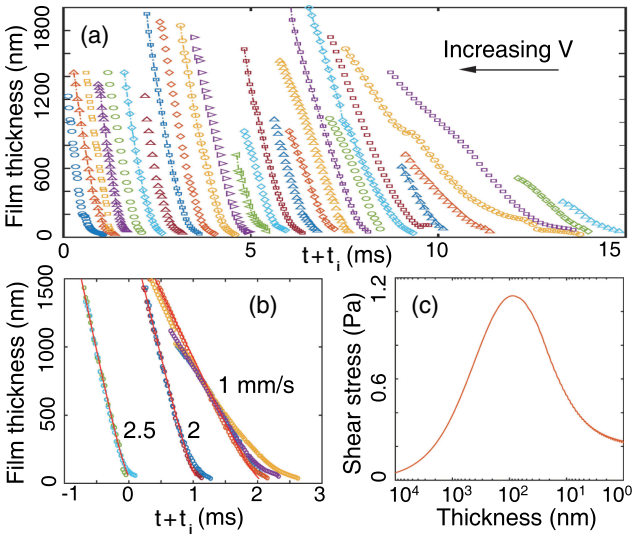

FIG. 3. (a) Experimental film drainage at different approach velocities in the range 0.5 to 2.8 mm/s. The slope of thickness-time evolution indicates the film thinning velocity. (b) Comparison between experiments and theory [20,21,23] that assumes lubrication and fully mobile boundary conditions. In (a) and (b) each curve "i" has been shifted by a time t_i for clarity. (c) In the theoretical prediction, the maximum shear stress along the interfaces evolves with center film thickness ($R_s = 0.65$ mm, $V = 10$ mm/s).

Comparisons between the model and the experimental results are shown in Fig. 3(b). The rapid film thinning behavior is successfully captured in the prediction; therefore, the negligible resistance during collision can be explained by the low viscosity of the air phase [20]. Further information can be obtained from the simulation; e.g., the interfacial velocity U and shear stress τ_f at the interfaces are nonuniform with the maximum values found at the outer region of the formed thin liquid film.

Unfortunately, the model predicted faster drainage rates than the experiment at thicknesses smaller than ~100 nm (see Fig. S4 in the Supplemental Material [23]). The predicted film thinning speed did not slow down until a film thickness at ~30 nm was reached. One possible explanation for the discrepancy is the existence of a Marangoni stress $\partial\sigma/\partial r$ at the interface, which was neglected in the model but could resist τ_f in the experiment. The air-water interface is known to be easily contaminated by surface active impurities [6,25]. Because of the continuous convection flow that sweeps the impurities out, the surface tension gradient along the interface can increase during the film thinning process.

In this scenario, the interfacial velocity U would be jointly determined by the Marangoni stress and the shear stress using the relationship $\tau_b = \partial\sigma/\partial r + \tau_f$. According to the theoretical prediction shown in Fig. 3(c), the maximum shear stress along the surface evolves with film thickness and has a peak of around 1 Pa at a film thickness

close to 100 nm. Marangoni stress ($\Delta\sigma/\Delta r$) at the same magnitude is easily achieved by a surface tension gradient ($\Delta\sigma$) of around 0.1 mN/m from the center to the outer region (assuming a characteristic radius Δr of 100 μm) of the thin liquid film. Therefore, the slowdown of the film thinning rate at small film thickness (large $\partial\sigma/\partial r$), which is more obvious at low collision speeds (small τ_f), is a consequence of the Marangoni stress. This effect can also explain experimental results with immobile boundary conditions ($|\tau_f| = |\partial\sigma/\partial r|$) [8,17,22], inward flow of the thin liquid film ($|\tau_f| < |\partial\sigma/\partial r|$) [26], and rapid bubble coalescence, within milliseconds, with high collision velocities and/or clean water ($|\tau_f| > |\partial\sigma/\partial r|$) [3,7,27].

To further understand the role of Marangoni stress on surface mobility, surfactant was added in water to change the interfacial tension in a controlled manner. The ionic surfactant sodium dodecyl sulfate (SDS, Sigma Aldrich) was used at very diluted concentrations (5, 7.5, 10, and 15 μM). Considering the dynamic adsorption process, the freshly generated bubbles were allowed to age for 10 min before the collision, with a measured interfacial tension change ($\Delta\sigma$) smaller than 0.2 mN/m (Krüss k12, ring method) when compared to pure water. In these diluted SDS solutions, the colliding bubbles exhibited two main outcomes: (i) Bubbles coalesced within a few milliseconds (< 5 ms), which will be referred to hereafter as "rapid coalescence"; (ii) bubbles took a much longer time to coalesce or did not coalesce after an experimental period of 20 sec, which feature the formation of a dimple [Fig. 4(a)] from which the liquid drained slowly until an equilibrium thin liquid film formed. This film was stabilized by the negatively charged air-water interfaces with the estimated surface potential of -80 ± 20 mV.

The impact of Marangoni stress was clearly demonstrated by the immobilization of the air water interfaces in the second case. This effect was also manifested in cases with short coalescence time in various ways. For example, the radius of thin liquid films before rupture, which was very small for clean water [~30 μm, Fig. 4(b)], became much larger with the addition of SDS [~100 μm, Figs. 4(a) and 4(c)], indicating an increase in the resistance at the interfaces. More significantly, the snapshots for 10 μM SDS shown in Fig. 4(c) describe the formation of a dimple during the early stage, which diminished rapidly and ruptured in milliseconds. By analyzing the complete fringes [4,7], film profiles are presented in Fig. 4(d). The formation of the dimple clearly indicates that the interfaces were initially immobile; however, the subsequent rapid film thinning in milliseconds suggests that the boundary condition changed to mobile during the film thinning process. This transition can be explained by the lesser impact of the Marangoni stress when compared to the increasing shear stress in the dynamic process.

The approach velocities ranging from 1 to 50 mm/s would change the maximum shear stress at the immobile interface following the relationship $\tau_{\mathrm{fmax}} \approx 0.5 Ca^{0.25}\sigma/R$ ($Ca = \mu V/\sigma$, with μ the water viscosity) [22]. The probability of rapid coalescence as a function of the maximum shear stress (assume $R_s = 0.65$ mm) is presented in Fig. 4(e) for SDS concentrations of 5, 7.5, 10, and 15 μM. The probabilities were generated after at least 20 repeated experiments for each case. Consistent noncoalescence was observed at low shear stress ($|\partial\sigma/\partial r| \geq |\tau_f|$, low approach velocity), and consistent quick coalescence at large shear stress ($|\partial\sigma/\partial r| < |\tau_f|$, large approach velocity). For values in between, the experimental outcomes appeared to follow a probabilistic behavior and were reasonably fitted by the cumulative Gaussian distribution function. As the SDS concentration was increased, faster approach velocities were required for rapid coalescence; moreover, rapid coalescence was not observed for 15 μM, illustrating that the Marangoni stress would be dominant over the shear stress at this concentration or larger. In the great majority of scenarios, the film would either be ruptured in milliseconds or be stabilized, a result that agrees well with the prediction of Chesters [28] that the surfactant would either completely immobilize the surface or be driven away by the film flow.

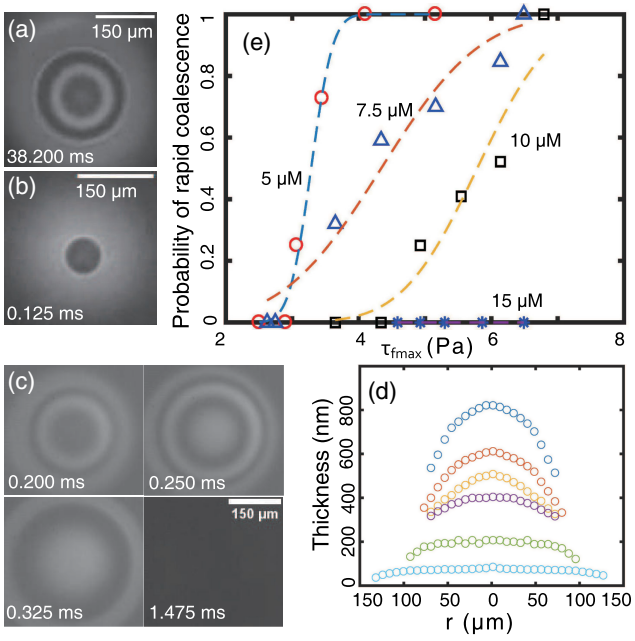

FIG. 4. (a) Fringes showing dimple formation in 7.5 μM SDS solution, $R_s = 0.83$ mm, $V = 2.8$ mm/s ($\tau_{\mathrm{fmax}} \approx 3.2$ Pa). (b) Small film width in pure water, $R_s = 0.85$ mm, $V = 2.8$ mm/s. (c) Rapid evolution of interference fringes in 10 μM SDS, $R_s = 0.79$ mm, $V = 50$ mm/s ($\tau_{\mathrm{fmax}} \approx 6.6$ Pa), resulting in (d) film profiles for times from top to bottom: 0.175, 0.250, 0.300, 0.350, 0.500, and 1.325 ms. (e) The probability of rapid coalescence (< 5 ms) as a function of maximum shear stress ($\tau_{\mathrm{fmax}} \sim V^{0.25}$, symbols), where "0" represent no coalescence and "1" represents rapid coalescence. Lines correspond to a cumulative Gaussian distribution fit.

In summary, we investigated the thin film drainage between two quickly colliding bubbles using high speed interferometry. The experimental results in the clean water system provided rapid film thinning rates almost identical to the collision speeds, indicating negligible resistance and mobile hydrodynamic boundary condition at the air-water interface. Results in the presence of a small amount of surfactant, which changed the interfacial tension in the order of 10^{-4} N/m, highlighted the role of the Marangoni stress caused by the uneven distribution of surface active materials in the hydrodynamic boundary condition. The Marangoni stress can balance the shear stress, hindering the mobility of the air-water interface and even resulting in a transition from a mobile to an immobile boundary condition. The competition between stresses might evolve continually over the thinning process for the mobile interface, but once balance has been achieved, the surface becomes immobile. Our systematic investigation provides explanations for previous experimental data that had either fast or slow bubble coalescence.

We wish to acknowledge the financial support of the Natural Science and Engineering Research Council of Canada and the Canadian Centre for Clean Coal/Carbon and Mineral Processing Technology (C5MPT). Suggestions by Professor Amy P. Tsai are greatly appreciated.

*qingxia2@ualberta.ca

[1] R. A. Verschoof, R. C. A. van der Veen, C. Sun, and D. Lohse, Phys. Rev. Lett. **117**, 104502 (2016).
[2] R. H. Yoon, Miner. Eng. **6**, 619 (1993).
[3] R. G. Horn, L. A. Del Castillo, and S. Ohnishi, Adv. Colloid Interface Sci. **168**, 85 (2011).
[4] B. Liu, R. Manica, X. Zhang, A. Bussonnière, Z. Xu, G. Xie, and Q. Liu, Langmuir **34**, 11667 (2018).
[5] R. Kirkpatrick and M. Lockett, Chem. Eng. Sci. **29**, 2363 (1974).
[6] D. Langevin, Curr. Opin. Colloid Interface Sci. **20**, 92 (2015).
[7] V. V. Yaminsky, S. Ohnishi, E. A. Vogler, and R. G. Horn, Langmuir **26**, 8061 (2010).
[8] I. U. Vakarelski, R. Manica, E. Q. Li, E. S. Basheva, D. Y. C. Chan, and S. T. Thoroddsen, Langmuir **34**, 2096 (2018).
[9] I. U. Vakarelski, R. Manica, X. Tang, S. J. O'Shea, G. W. Stevens, F. Grieser, R. R. Dagastine, and D. Y. Chan, Proc. Natl. Acad. Sci. U.S.A. **107**, 11177 (2010).
[10] D. Schäffel, K. Koynov, D. Vollmer, H.-J. Butt, and C. Schönecker, Phys. Rev. Lett. **116**, 134501 (2016).
[11] P. Tsai, A. M. Peters, C. Pirat, M. Wessling, R. G. Lammertink, and D. Lohse, Phys. Fluids **21**, 112002 (2009).
[12] I. U. Vakarelski, E. Klaseboer, A. Jetly, M. M. Mansoor, A. A. Aguirre-Pablo, D. Y. C. Chan, and S. T. Thoroddsen, Sci. Adv. **3**, e1701558 (2017).
[13] A. K. Chesters and G. Hofman, in *Mechanics and Physics of Bubbles in Liquids* (Springer, New York, 1982), pp. 353–361.
[14] L. A. Del Castillo, S. Ohnishi, and R. G. Horn, J. Colloid Interface Sci. **356**, 316 (2011).
[15] M. H. W. Hendrix, R. Manica, E. Klaseboer, D. Y. C. Chan, and C. D. Ohl, Phys. Rev. Lett. **108**, 247803 (2012).
[16] L. Parkinson and J. Ralston, J. Phys. Chem. C **114**, 2273 (2010).
[17] D. Y. C. Chan, E. Klaseboer, and R. Manica, Adv. Colloid Interface Sci. **165**, 70 (2011).
[18] X. Zhang, P. Tchoukov, R. Manica, L. Wang, Q. Liu, and Z. Xu, Soft Matter **12**, 9105 (2016).
[19] Y. Gao and L. Pan, Langmuir **34**, 14215 (2018).
[20] R. H. Davis, J. A. Schonberg, and J. M. Rallison, Phys. Fluids A **1**, 77 (1989).
[21] S. Abid and A. K. Chesters, Int. J. Multiphase Flow **20**, 613 (1994).
[22] E. Klaseboer, J. P. Chevaillier, C. Gourdon, and O. Masbernat, J. Colloid Interface Sci. **229**, 274 (2000).
[23] See Supplemental Material at http://link.aps.org/supplemental/10.1103/PhysRevLett.122.194501 for details on the bubble generation, interferometry method, model description. and prediction. Three movies show (i) simultaneous observation of side view bubble collision and bottom view interference fringes, (ii) slow drainage and equilibrium film, and (iii) interference fringes describing transition from the immobile to mobile boundary condition.
[24] V. V. Yaminsky, S. Ohnishi, E. A. Vogler, and R. G. Horn, Langmuir **26**, 8075 (2010).
[25] A. Maali, R. Boisgard, H. Chraibi, Z. Zhang, H. Kellay, and A. Würger, Phys. Rev. Lett. **118**, 084501 (2017).
[26] X. Zhang, R. Manica, P. Tchoukov, Q. Liu, and Z. Xu, J. Phys. Chem. C **121**, 5573 (2017).
[27] L. A. Del Castillo, S. Ohnishi, S. L. Carnie, and R. G. Horn, Langmuir **32**, 7671 (2016).
[28] A. K. Chesters and I. B. Bazhlekov, J. Colloid Interface Sci. **230**, 229 (2000).